Atom Interferometry in an Optical Cavity

Paul Hamilton,[*] Matt Jaffe, Justin M. Brown,[†] Lothar Maisenbacher,[‡] Brian Estey, and Holger Müller[§]
Department of Physics, University of California, Berkeley, California 94720, USA
(Received 24 September 2014; published 11 March 2015)

We propose and demonstrate a new scheme for atom interferometry, using light pulses inside an optical cavity as matter wave beam splitters. The cavity provides power enhancement, spatial filtering, and a precise beam geometry, enabling new techniques such as low power beam splitters ($< 100\ \mu$W), large momentum transfer beam splitters with modest power, or new self-aligned interferometer geometries utilizing the transverse modes of the optical cavity. As a first demonstration, we obtain Ramsey-Raman fringes with $> 75\%$ contrast and measure the acceleration due to gravity, g, to 60 $\mu g/\sqrt{\text{Hz}}$ resolution in a Mach-Zehnder geometry. We use $> 10^7$ cesium atoms in the compact mode volume (600 μm $1/e^2$ waist) of the cavity and show trapping of atoms in higher transverse modes. This work paves the way toward compact, high sensitivity, multiaxis interferometry.

DOI: 10.1103/PhysRevLett.114.100405 PACS numbers: 03.75.Dg, 06.30.Gv, 37.25.+k, 37.30.+i

In a light-pulse atom interferometer, recoils from photon-atom interactions are used to split and interfere matter waves (see Fig. 1). These interferometers have been used to measure the gravitational acceleration $\vec{g}$ [1], rotation $\vec{\Omega}$ [2], gravity gradients [3], the fine structure constant [4], Newton's gravitational constant [5,6], and absolute masses in a proposed revision of the SI [7,8], to test Einstein's equivalence principle [9–12], and have been proposed to measure the free fall of antimatter [13] and to detect gravitational waves [14–16]. The sensitivity of a conventional Mach-Zehnder interferometer increases with the measured phase difference

$$\phi = \{2\vec{\Omega} \cdot [\vec{k}_{\text{eff}} \times (\vec{v}_0 + \vec{g}T)] + \vec{k}_{\text{eff}} \cdot \vec{g}\}T^2 \qquad (1)$$

(where $\vec{v}_0$ is the initial velocity of the atom), which scales with the pulse separation time T and the recoil momentum $\vec{p} = \hbar\vec{k}_{\text{eff}}$, where $\vec{k}_{\text{eff}}$ is the effective wave number of the photons. State of the art atom interferometers are limited by several engineering boundaries. T is limited by the free-fall time in atomic fountains, which are now as high as 10 m [17,18]. Multiphoton interactions can increase the recoil momentum to a multiple $n\hbar k$ of the single photon recoil [19–23] but are limited by the available laser power (e.g., 6 W in [24], 43 W in [25]). Finally, wave front distortions spread the local wave vector around its mean, lowering interference contrast and reducing both sensitivity and accuracy. An optical cavity can solve these problems by providing spatial filtering to clean the wave fronts and enhancing laser intensity. However, running an atom interferometer inside an optical cavity presents challenges in keeping the atoms in the relatively small cavity mode volume and having multiple laser frequencies (needed due to recoil frequency shifts, Doppler shifts, and atomic structure) simultaneously resonant with the cavity. Here, we present a cesium atom interferometer inside an in-vacuum optical cavity and demonstrate gravity measurements using less than 100 μW of laser power incident on the cavity.

The use of an optical cavity has many advantages. First, laser power limits interferometers using both large momentum transfer beam splitters and optical lattices. For example, Bragg diffraction requires an intensity proportional to n^2 for constant pulse duration, or n^4 for a constant single-photon scattering rate at an increased detuning [26]. With resonant enhancement in a cavity, we may achieve $n = 50$–100 photon Bragg transitions using tens of milliwatts of power from a standard diode laser as opposed to the multiple watt systems recently developed [24,25]. Similarly, we can reduce scattering from optical lattices by using increased intensity at a larger detuning.

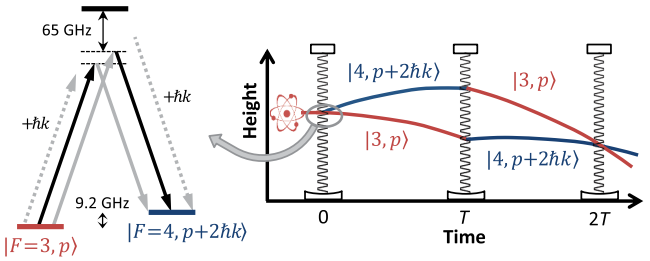

FIG. 1 (color online). Left: Energy level scheme. A two-photon Raman interaction between the ground hyperfine states of cesium transfers momentum to the atoms. The laser (black arrows) is modulated at the hyperfine frequency creating sidebands (gray arrows). Two resonant pathways (solid arrows) can interfere depending on the position of the atoms and the detuning from an optical cavity resonance. Right: Mach-Zehnder interferometer. Momentum transfer from three pulses of a laser standing wave (wavy black lines) separated by a time T split, redirect, and interfere a matter wave (red and blue lines).

Second, uncontrolled spatial variations in the laser amplitude and phase (e.g., speckle from imperfect optical surfaces) can reduce interferometric contrast in free fall interferometers or cause unwanted forces in schemes which use an optical lattice to hold atoms [27,28]. An optical cavity spatially filters the interferometry beam giving smooth optical phase fronts which vary in a calculable manner.

Third, interferometer geometries with enclosed spatial area typically use independent laser beams, whose relative vibration and alignment need to be tightly controlled. Using multiple transverse spatial modes of the optical cavity provides self-aligned interferometry beams. In addition, multiple simultaneous interferometers could provide common-mode rejection of vibrational noise in rotation measurements.

Fourth, many systematics, e.g., gravity gradients, electric and magnetic fields and gradients, are more easily controlled in a small volume. The combination of large momentum transfer and long coherence times in an optical lattice provides high sensitivity in a compact area.

Finally, the position uncertainty typical in atomic fountains, optical wave front curvature, and Gouy phase shifts are leading systematics in precision experiments [4–7]. The well-defined geometry of the optical cavity reduces them. Counterpropagation of the interferometry beams is also intrinsic in an optical cavity. Optical beam parameters can be determined precisely by measuring the transverse mode spacing of the cavity.

Our experiment uses a two-dimensional magneto-optical trap (2D-MOT) to feed a 3D-MOT through a differential pumping stage. A vacuum of below 10^{-9} Torr is maintained inside the main vacuum chamber. All frequencies are stabilized ("locked") to a reference laser, which is in turn stabilized to the cesium D_2 transition at 852 nm by modulation transfer spectroscopy. An experimental run starts with loading $\approx 5 \times 10^8$ cesium atoms into the 3D-MOT in one second. After increasing the detuning of the 3D-MOT beams from -1.5 to -12 linewidths ($\Gamma = 2\pi \times 5.2$ MHz) and decreasing the optical power, polarization gradients cool the atoms in the $F = 4$ state to 6 μK.

For operation of the interferometer, both frequencies needed to drive Raman or Bragg transitions (the "science laser") must be kept on resonance with the "science" cavity surrounding our interferometer. We use a second "tracer" laser with a wavelength of 780 nm to stabilize the length of the science cavity. The large detuning and low intensity (<50 μW incident on the cavity) along with a reduced cavity finesse of ≈ 30 at 780 nm lead to a single photon scattering rate of ≈ 1 μHz. The spatial gradient of the ac Stark shift ($\approx h \times 8$ Hz) due to diffraction of the tracer laser causes a negligible force of 2×10^{-14} g on the atoms. Both lasers are locked to an external transfer cavity whose length is stabilized to the reference laser (see Fig. 2). Before going

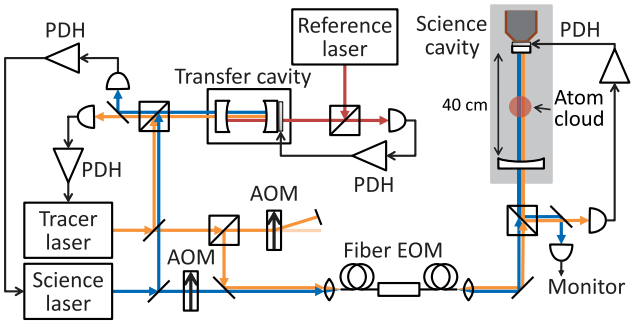

FIG. 2 (color online). Cavity and laser frequency stabilization. An external transfer cavity acts as a common reference for both the science laser and a second far-detuned laser (the "tracer" laser) which is used to stabilize the science cavity inside the vacuum chamber (gray box). The transfer cavity itself is stabilized to a reference laser. Cavity lengths and laser frequencies are stabilized via feedback using the Pound-Drever-Hall (PDH) method.

to the science cavity, the tracer laser is double-passed through a 200 MHz bandwidth acousto-optic modulator (AOM, Brimrose TEF-300-200-0.780) which is tuned such that both lasers are simultaneously resonant with both cavities. Feedback to the science cavity is applied to a piezo-driven $1/2''$ diameter flat gold mirror with a feedback bandwidth of 40 kHz [29]. The other cavity mirror has a $1''$ diameter and 5 m radius of curvature. The fundamental longitudinal mode of the cavity has a beam waist of 600 μm located at the surface of the flat mirror, a finesse of ≈ 150, and a linewidth of 2.5 MHz. The transverse modes of the cavity are nondegenerate in resonance frequency. For the demonstrations below, where the laser is tuned to only couple strongly to the fundamental mode of the cavity, the incoming interferometry beam is, thus, effectively spatially filtered.

The length of the cavity (40.756 cm) was chosen to be nearly an integer number of half wavelengths of the ground state hyperfine splitting (HFS) $\nu_{\mathrm{HFS}} = 9192631770$ Hz of cesium. This allows the two science-laser frequencies needed for Raman transitions to be simultaneously near resonant with the cavity mode. They are generated from a single laser by a fiber coupled broadband electro-optic modulator (EOM). Low phase noise of this frequency is crucial, as it directly enters the measured phase of the interferometer. We use a dielectric resonator oscillator locked to a harmonic of a low-noise quartz crystal. Low phase noise is achieved by using a nonlinear transmission line (Picosecond Pulse Labs) as a harmonic generator. For Bragg diffraction and Bloch oscillations, the science laser passes through an AOM which can be modulated at two frequencies [30].

We coarsely select atoms from the MOT that are located in the science cavity mode by first turning on the science laser, detuned ≈ -65 GHz from the D_2 transition at 852 nm, to create an optical lattice. Atoms not located

in the lattice or with too high temperature fall away, leaving 2×10^8 atoms. The temperature transverse to the cavity mode increases to 25 μK as the atoms are loaded into the lattice, but the longitudinal temperature is reduced to <2 μK upon release from the lattice, most likely by adiabatic expansion. We then optically pump $> 75\%$ of the atoms to the magnetically insensitive $F = 4$, $m_F = 0$ sublevel by applying a magnetic bias field of 140 mG and a retroreflected beam resonant with the $F = 4 \rightarrow F' = 4$ transition with linear polarization parallel to the bias field. A small amount of repump light on the $F = 3 \rightarrow F' = 4$ transition is simultaneously applied. For both state and spatial selection, we apply a series of Raman pulses on the $F = 3$, $m_F = 0 \leftrightarrow F = 4$, $m_F = 0$ clock transition. Each pulse is followed by a clearing beam (either on the cycling $F = 4 \rightarrow F' = 5$ or $F = 3 \rightarrow F' = 2$ transitions). This both removes atoms that were not initially in the $m_F = 0$ sublevel and preferentially selects atoms towards the center of the cavity mode. Without this spatial selection the widths of the atomic distribution and optical interferometry beams are initially similar, and we can achieve a maximum population transfer of only $\approx 50\%$ with low contrast on Rabi oscillations. Modeling the effect of intensity variations across the cavity mode can explain this observed contrast. However, using three state selection pulses with a length that maximizes population inversion at the center of the cavity mode allows us to reach 90% population transfer (see Fig. 3, top).

Use of an EOM to generate the Raman frequency pair is a simple way to reach low phase noise, but leads to two sidebands of equal amplitude and opposite phase [31]. At detunings large compared to the hyperfine structure of the excited state, the two pairs of a sideband and the carrier drive Raman transitions (see Fig. 1, left) which interfere with a position dependent phase. Because the hyperfine splitting is ≈ 2.2 MHz off (similar to the science cavity linewidth) from being a multiple of the free spectral range of the science cavity, we may selectively enhance one pair of a sideband and the carrier while suppressing the other, preventing this cancellation.

We now present experiments that lead up to our demonstration of intracavity atom interferometry: velocity-insensitive and -sensitive Raman pulses, a Raman-Ramsey sequence, and, finally, atom interferometry measuring the acceleration due to free fall, g. Raman transitions using a copropagating pair of photons are velocity insensitive and transfer negligible momentum to the atoms. We optically drive a combination of two such Raman $\pi/2$ pulses between the clock states $F = 3$, $m_F = 0 \rightarrow F = 4$, $m_F = 0$, spaced by a pulse separation time of T $= 2$ ms to generate the Ramsey fringes shown in Fig. 4. The high contrast demonstrates the good coherence of the process despite the comparable size of the atomic cloud and interferometry beams. This measurement is an optical version of a cesium fountain clock. The optical

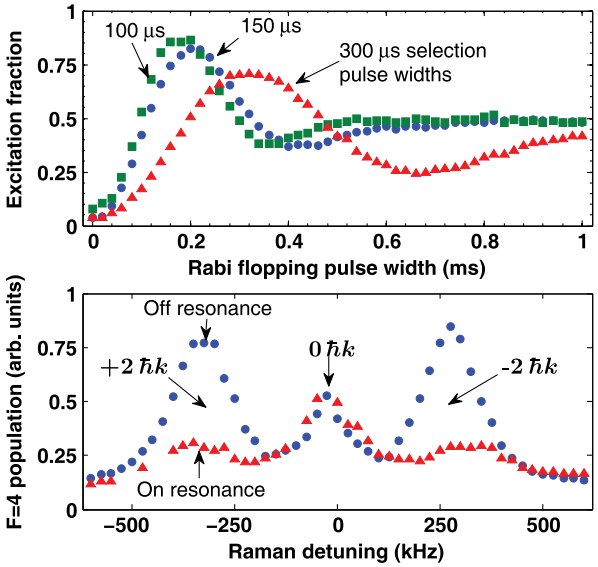

FIG. 3 (color online). Top: Rabi flopping on the velocity insensitive transition after three state selection pulses with fixed intensity having pulse widths of 300 μs (red), 150 μs (blue), and 100 μs (green), followed by clearing pules shows improved contrast as atoms near the center of the cavity mode are preferentially selected. Bottom: Cavity suppression of velocity sensitive transitions. Changing the cavity length to be either on resonance with the carrier (red) or 2.2 MHz off resonance (blue) emphasizes one carrier-sideband pair and prevents cancellation of the transition amplitude.

pulses lead to an ac Stark shift of the transition frequency (e.g., -2.35 kHz in Fig. 4). By varying the optical intensity while keeping the pulse area constant we find an extrapolated value for the transition frequency at zero intensity of 9 192 631 590(50) Hz. With microwave pulses, we find that, after a 10 Hz correction due to the quadratic Zeeman effect, the measured transition frequency of 9 192 631 770 (1) Hz agrees with the international definition of the second.

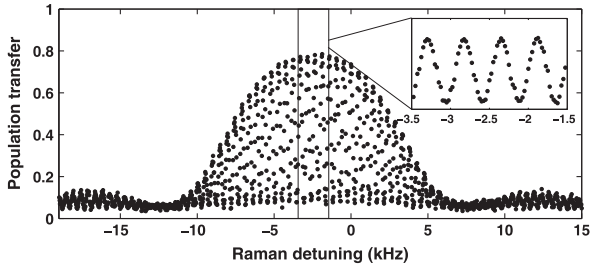

FIG. 4. Raman-Ramsey fringes. Two Raman $\pi/2$ pulses on the cesium clock transition are applied with a separation time $T = 2$ ms. Each point is the average from four experimental runs. The high contrast and signal-to-noise ratio of the fringes demonstrates that, despite the small size of the optical cavity mode waist, spatial selection of the atoms gives a uniform Rabi frequency for the 2×10^7 atoms participating in the interferometer sequence.

Next, we demonstrate velocity-sensitive Raman pulses (using counterpropagating pairs of photons) that transfer a momentum of $\pm 2\hbar k$ (Fig. 3, bottom). The falling atoms cause a Doppler shift of the velocity-sensitive transitions which allows us to suppress the unwanted velocity-insensitive transition. As discussed above, detuning the cavity resonance to suppress one EOM sideband further enhances the velocity-sensitive transition probability by a factor of 3.

Finally, we demonstrate atom interferometry and perform a gravity measurement by a $\pi/2 - \pi - \pi/2$ combination of three velocity sensitive Raman pulses, which constitutes a Mach-Zehnder interferometer. To remain resonant as the freely falling atoms accelerate, the difference frequency in the Raman frequency pair is swept at a rate of $k_{\text{eff}} a_{\text{eff}}$ ($\approx 2\pi \times 23$ MHz s^{-1} for $a = 9.8$ ms^{-2}). We detect the interferometer outputs separately by first pushing atoms in either $F = 4$ or $F = 3$ to the side with our clearing beams and then using fluorescence detection on a CCD camera to spatially resolve the two populations. After normalization to take out atom-number fluctuations, we obtain the interference fringes shown in Fig. 5 by scanning the rate of the frequency ramp. When the frequency ramp matches the acceleration, the interferometer phase, $k_{\text{eff}}(g - a_{\text{eff}})T^2$, should be zero independent of the pulse separation time T. At a maximum pulse separation time $T = 15$ ms we achieve a resolution of 60 $\mu g/\sqrt{\text{Hz}}$, similar to the sensitivity achieved by other compact atom interferometers [32]. Additionally, we find that, with as little as 87 μW of power, and at a smaller single photon detuning of 2 GHz, we attain fringes with $>10\%$ contrast for $T = 1$ ms.

We have demonstrated the first atom interferometer in an optical cavity. We have shown that tuning the cavity resonance allows us to selectively address both velocity-sensitive and -insensitive transitions as well as to choose the direction of the momentum kicks in the interferometer, a technique that can be used to reverse many systematic effects. Atoms have been loaded efficiently into the fundamental cavity mode. The setup uses diode lasers only. Using sidebands generated by a wideband EOM to drive Raman transitions avoids the noise usually contributed by a laser phase lock and is possible without undue systematic effects thanks to the cavity's rejection of the unwanted sideband. Despite the small size of the cavity mode, we achieved high contrast using optical beam splitters.

While this proof-of-principle demonstration relied on hyperfine changing Raman transitions, we expect, with the power enhancement of the optical cavity, that large momentum transfer multiphoton Bragg beam splitters will be possible [26]. For the future, the combination of very large momentum transfer and short pulse separation times will make a compact setup which is less sensitive to low-frequency vibrations. Localization of atoms in the cavity, and precise control of the mode of the laser beam should help suppress major systematics in measurements of the fine structure constant, a proposed mass standard [7], the gravitational constant [5,6], or deviations from Newtonian gravity at short distances [33]. With these beam splitters and far-detuned intracavity optical lattices, which can have negligible single-photon scattering, we plan on exploring a range of applications from inertial sensors [34] to the first measurement of the gravitational analog of the Aharonov-Bohm effect [35]. For example, in Fig. 6, we show one possible realization of a rotational sensor utilizing self-aligned transverse modes of the cavity and a demonstration of atoms loaded into such modes. Recently developed methods for both preparing and detecting spin squeezed states [36,37] in a similar optical cavity could lead to improved sensitivity beyond the standard quantum limit. Use of the cavity mode itself to detect intracavity matter wave interference could even allow for nondemolition continuous force detection as proposed in [38,39]. In addition, the compact size and low power requirements make a cavity interferometer ideal for future mobile or space-based applications [40]. Finally, the techniques

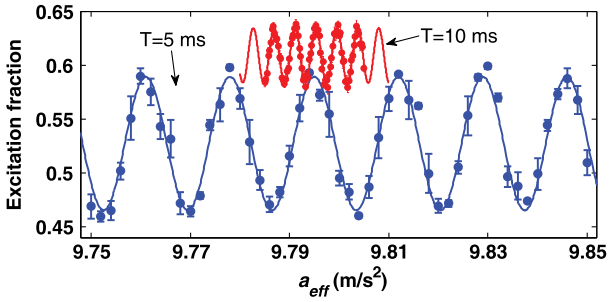

FIG. 5 (color online). Mach-Zehnder fringes of a $\pi/2 - \pi - \pi/2$ pulse sequence on the cesium clock transition with pulse separation times $T = 5$ ms (blue) and $T = 10$ ms (red). The Raman frequency difference is linearly ramped to give an effective acceleration, a_{eff}, which compensates for the Doppler shift from the acceleration due to gravity. The phase of the interferometer is given by $k_{\text{eff}}(g - a_{\text{eff}})T^2$.

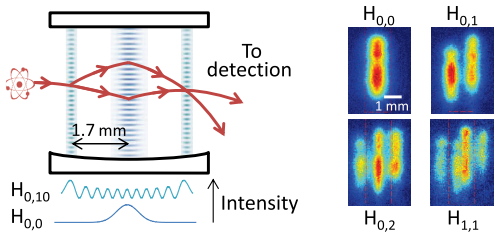

FIG. 6 (color online). Left: A possible implementation of a rotation sensitive interferometer enclosing a spatial area using transverse cavity modes. Atoms enter the cavity from the side and are split by a pulsed standing wave in the Hermite-Gaussian $H_{0,10}$ cavity mode, reflected by a pulse in the fundamental $H_{0,0}$ mode, and interfered on the far side with a second pulse of the $H_{0,10}$ mode. Right: Fluorescence images of atoms in optical lattices formed by transverse modes of the optical cavity.

discussed here may be of interest to proposed experiments using optical cavities to enhance diffraction in systems without easily accessible resonant transitions, e.g., macroscopic masses [41] or antihydrogen [13].

We thank Q. Simmons and T. Gavrilchenko for their contributions to the apparatus and P. Haslinger, D. Schlippert, and C. Thomas for their comments on the manuscript. J. M. B. thanks the Miller Institute for Basic Research in Science for support. This work has been supported by the David and Lucile Packard Foundation, the Defense Advanced Research Projects Agency, the National Aeronautics and Space Agency Grants No. NNH13ZTT002N, No. NNH10ZDA001N-PIDDP, and No. NNH11ZTT001N, and the National Science Foundation Grant No. 1404566.

*paul.hamilton@berkeley.edu
†C.S. Draper Laboratory, Inc., 555 Technology Square, Cambridge, Massachusetts 02139, USA.
‡Max-Planck-Institut für Quantenoptik, 85748 Garching, Germany.
§Also at Lawrence Berkeley National Laboratory, One Cyclotron Road, Berkeley, California 94720, USA.

[1] A. Peters, K. Y. Chung, and S. Chu, High-precision gravity measurements using atom interferometry, Metrologia **38**, 25 (2001).
[2] D. S. Durfee, Y. K. Shaham, and M. A. Kasevich, Long-Term Stability of an Area-Reversible Atom-Interferometer Sagnac Gyroscope, Phys. Rev. Lett. **97**, 240801 (2006).
[3] J. M. McGuirk, G. T. Foster, J. B. Fixler, M. J. Snadden, and M. A. Kasevich, Sensitive absolute-gravity gradiometry using atom interferometry, Phys. Rev. A **65**, 033608 (2002).
[4] R. Bouchendira, P. Cladé, S. Guellati-Khélifa, F. Nez, and F. Biraben, New Determination of the Fine Structure Constant and Test of the Quantum Electrodynamics, Phys. Rev. Lett. **106**, 080801 (2011).
[5] J. B. Fixler, G. T. Foster, J. M. McGuirk, and M. A. Kasevich, Atom interferometer measurement of the Newtonian constant of gravity, Science **315**, 74 (2007).
[6] G. Rosi, F. Sorrentino, L. Cacciapuoti, M. Prevedelli, and G. M. Tino, Precision measurement of the Newtonian gravitational constant using cold atoms, Nature (London) **510**, 518 (2014).
[7] S.-Y. Lan, P.-C. Kuan, B. Estey, D. English, J. M. Brown, M. A. Hohensee, and H. Müller, A clock directly linking time to a particle's mass, Science **339**, 554 (2013).
[8] R. Bouchendira, P. Cladé, S. Guellati-Khélifa, F. Nez, and F. Biraben, State of the art in the determination of the fine structure constant: test of Quantum Electrodynamics and determination of h/m_u, Ann. Phys. (Berlin) **525**, 484 (2013).
[9] S. Fray, C. A. A. Diez, T. W. Hänsch, and M. Weitz, Atomic Interferometer with Amplitude Gratings of Light and Its Applications to Atom Based Tests of the Equivalence Principle, Phys. Rev. Lett. **93**, 240404 (2004).
[10] A. Bonnin, N. Zahzam, Y. Bidel, and A. Bresson, Simultaneous dual-species matter-wave accelerometer, Phys. Rev. A **88**, 043615 (2013).
[11] M. G. Tarallo, T. Mazzoni, N. Poli, D. V. Sutyrin, X. Zhang, and G. M. Tino, Test of Einstein Equivalence Principle for 0-Spin and Half-Integer-Spin Atoms: Search for Spin-Gravity Coupling Effects, Phys. Rev. Lett. **113**, 023005 (2014).
[12] D. Schlippert, J. Hartwig, H. Albers, L. L. Richardson, C. Schubert, A. Roura, W. P. Schleich, W. Ertmer, and E. M. Rasel, Quantum Test of the Universality of Free Fall, Phys. Rev. Lett. **112**, 203002 (2014).
[13] P. Hamilton, A. Zhmoginov, F. Robicheaux, J. Fajans, J. S. Wurtele, and H. Müller, Antimatter Interferometry for Gravity Measurements, Phys. Rev. Lett. **112**, 121102 (2014).
[14] S. Dimopoulos, P. W. Graham, J. M. Hogan, M. A. Kasevich, and S. Rajendran, Atomic gravitational wave interferometric sensor, Phys. Rev. D **78**, 122002 (2008).
[15] J. Harms, B. J. J. Slagmolen, R. X. Adhikari, M. C. Miller, M. Evans, Y. Chen, H. Müller, and M. Ando, Low-frequency terrestrial gravitational-wave detectors, Phys. Rev. D **88**, 122003 (2013).
[16] B. Barrett, P. A. Gominet, E. Cantin, L. Antoni-Micollier, A. Bertoldi, B. Battelier, P. Bouyer, J. Lautier, and A. Landragin, Mobile and remote inertial sensing with atom interferometers, *Proceedings of the International School of Physics "Enrico Fermi", Course 188, Atom Interferometry*, edited by G. M. Tino and M. A. Kasevich (IOS Press, Amsterdam, 2014).
[17] A. Sugarbaker, S. M. Dickerson, J. M. Hogan, D. M. S. Johnson, and M. A. Kasevich, Enhanced Atom Interferometer Readout through the Application of Phase Shear, Phys. Rev. Lett. **111**, 113002 (2013).
[18] L. Zhou, Z. Y. Xiong, W. Yang, B. Tang, W. C. Peng, K. Hao, R. B. Li, M. Liu, J. Wang, and M. S. Zhan, Development of an atom gravimeter and status of the 10-meter atom interferometer for precision gravity measurement, Gen. Relativ. Gravit. **43**, 1931 (2011).
[19] H. Müller, S.-w. Chiow, Q. Long, S. Herrmann, and S. Chu, Atom Interferometry with up to 24-Photon-Momentum-Transfer Beam Splitters, Phys. Rev. Lett. **100**, 180405 (2008).
[20] S. W. Chiow, T. Kovachy, H.-C. C. Chien, and M. A. Kasevich, $102\hbar k$ Large Area Atom Interferometers, Phys. Rev. Lett. **107**, 130403 (2011).
[21] H. Müller, S. W. Chiow, S. Herrmann, and S. Chu, Atom Interferometers with Scalable Enclosed Area, Phys. Rev. Lett. **102**, 240403 (2009).
[22] P. Cladé, S. Guellati-Khélifa, F. Nez, and F. Biraben, Large Momentum Beam Splitter Using Bloch Oscillations, Phys. Rev. Lett. **102**, 240402 (2009).
[23] G. D. McDonald, C. C. N. Kuhn, S. Bennetts, J. E. Debs, K. S. Hardman, M. Johnsson, J. D. Close, and N. P. Robins, $80\hbar k$ momentum separation with Bloch oscillations in an optically guided atom interferometer, Phys. Rev. A **88**, 053620 (2013).
[24] S. W. Chiow, S. Herrmann, H. Müller, and S. Chu, 6W, 1kHz linewidth, tunable continuous-wave near-infrared laser, Opt. Express **17**, 5246 (2009).

[25] S. Chiow, T. Kovachy, J. M. Hogan, and M. A. Kasevich, Generation of 43 W of quasi-continuous 780 nm laser light via high-efficiency, single-pass frequency doubling in periodically poled lithium niobate crystals, Opt. Lett. **37**, 3861 (2012).

[26] H. Müller, S. W. Chiow, and S. Chu, Atom-wave diffraction between the Raman-Nath and the Bragg regime: Effective Rabi frequency, losses, and phase shifts, Phys. Rev. A **77**, 023609 (2008).

[27] P. Cladé, T. Plisson, S. Guellati-Khélifa, F. Nez, and F. Biraben, Theoretical analysis of a large momentum beamsplitter using Bloch oscillations, Eur. Phys. J. D **59**, 349 (2010).

[28] R. Charrière, M. Cadoret, N. Zahzam, Y. Bidel, and A. Bresson, Local gravity measurement with the combination of atom interferometry and Bloch oscillations, Phys. Rev. A **85**, 013639 (2012).

[29] T. C. Briles, D. C. Yost, A. Cingöz, J. Ye, and T. R. Schibli, Simple piezoelectric-actuated mirror with 180 kHz servo bandwidth, Opt. Express **18**, 9739 (2010).

[30] S. W. Chiow, S. Herrmann, S. Chu, and H. Müller, Noise-Immune Conjugate Large-Area Atom Interferometers, Phys. Rev. Lett. **103**, 050402 (2009).

[31] I. Dotsenko, W. Alt, S. Kuhr, D. Schrader, M. Müller, Y. Miroshnychenko, V. Gomer, A. Rauschenbeutel, and D. Meschede, Application of electro-optically generated light fields for Raman spectroscopy of trapped cesium atoms, Appl. Phys. B **78**, 711 (2004).

[32] H. J. McGuinness, A. V. Rakholia, and G. W. Biedermann, High data-rate atom interferometer for measuring acceleration, Appl. Phys. Lett. **100**, 011106 (2012).

[33] P. Wolf, P. Lemonde, A. Lambrecht, S. Bize, A. Landragin, and A. Clairon, From optical lattice clocks to the measurement of forces in the Casimir regime, Phys. Rev. A **75**, 063608 (2007).

[34] P. Hamilton, M. Jaffe, J. M. Brown, B. Estey, H. Müller, R. Compton, and K. Nelson, Concept of a miniature atomic sensor, *2014 International Symposium on Inertial Sensors and Systems (ISISS), Laguna Beach, California, 2014,* (IEEE, New York, 2014), pp. 1–4.

[35] M. A. Hohensee, B. Estey, P. Hamilton, A. Zeilinger, and H. Müller, Force-Free Gravitational Redshift: Proposed Gravitational Aharonov-Bohm Experiment, Phys. Rev. Lett. **108**, 230404 (2012).

[36] I. D. Leroux, M. H. Schleier-Smith, and V. Vuletić, Implementation of Cavity Squeezing of a Collective Atomic Spin, Phys. Rev. Lett. **104**, 073602 (2010).

[37] J. G. Bohnet, K. C. Cox, M. A. Norcia, J. M. Weiner, Z. Chen, and J. K. Thompson, Reduced spin measurement back-action for a phase sensitivity ten times beyond the standard quantum limit, Nat. Photonics **8**, 731 (2014).

[38] B. Prasanna Venkatesh, M. Trupke, E. A. Hinds, and D. H. J. O'Dell, Atomic Bloch-Zener oscillations for sensitive force measurements in a cavity, Phys. Rev. A **80**, 063834 (2009).

[39] B. M. Peden, D. Meiser, M. L. Chiofalo, and M. J. Holland, Nondestructive cavity QED probe of Bloch oscillations in a gas of ultracold atoms, Phys. Rev. A **80**, 043803 (2009).

[40] D. N. Aguilera *et al.*, STE-QUEST—test of the universality of free fall using cold atom interferometry, Classical Quantum Gravity **31**, 115010 (2014).

[41] P. Asenbaum, S. Kuhn, S. Nimmrichter, U. Sezer, and M. Arndt, 41) Cavity cooling of free silicon nanoparticles in high vacuum, Nat. Commun. **4**, 2743 (2013).